minerals

MDPI

Article

Filling Characteristics of Radiolarian Siliceous Shell Cavities at Wufeng-Longmaxi Shale in Sichuan Basin, Southwest China

Xiaofeng Zhou [1], Pingping Liang [2,*], Xizhe Li [2], Wei Guo [2], Xiaowei Zhang [2] and Jichen Yu [2]

[1] State Key Laboratory of Petroleum Resources and Prospecting, China University of Petroleum, Beijing 102249, China
[2] PetroChina Research Institute of Petroleum Exploration and Development, Beijing 100083, China
* Correspondence: liangpp69@petrochina.com.cn

Abstract: Both complete and uncompleted radiolarian siliceous shells were developed at Wufeng-Longmaxi radiolarian siliceous shale laminae in Sichuan Basin. Micro- and ultra-micropetrological observation suggests that they were successively filled by calcite, pyrite and organic–silicon complex, where pyrite and organic–silicon complex filled dissolved pores associated with calcite during sedimentation. Calcite was derived from calcium carbonate produced by microbial activities at the seawater surface. The environment of radiolarian siliceous shell cavities, which was suitable for sulfate reducing bacterial growth or dissolved hydrogen sulfide reducing Fe^{3+}, contributed positively to pyrite development. Organic–silicon complex development was related to microorganism metabolism that was an important silica source. Honeycomb-like organic pores were developed in cavities with complete shells, but were not developed in cavities with uncompleted shells. This is because the latter could not withstand overburden pressure compared with the former. The only approach to figure out organic pore carriers and understand sequences and development processes of minerals and organic matter is to select weakly compacted radiolarian siliceous shale laminae to carry out micro- and ultra-micropetrological observation and geochemical testing via various technologies.

Keywords: radiolarian siliceous shell cavity; fillings; genetic mechanism; organic pore carriers

Citation: Zhou, X.; Liang, P.; Li, X.; Guo, W.; Zhang, X.; Yu, J. Filling Characteristics of Radiolarian Siliceous Shell Cavities at Wufeng-Longmaxi Shale in Sichuan Basin, Southwest China. *Minerals* **2022**, *12*, 1545. https://doi.org/10.3390/min12121545

Academic Editor: Thomas Gentzis

Received: 4 November 2022
Accepted: 28 November 2022
Published: 30 November 2022

1. Introduction

Radiolarian silica, which is common and easily recognized in shale intervals, is an important source for biogenic silica. It has received considerable attention since it is a marker of high-quality shale reservoirs [1–8]. The radiolarian siliceous shell is generally round and oval in shape with enclosed space as a cavity. It is commonly characterized by "thin shell and large cavity", with shell thickness of 10–100 μm and cavity diameter of 30–250 μm. Fillings, e.g., calcite, pyrite, siliceous particles, etc., and organic matter with honeycomb-like pores, can be observed in cavities [9–13].

Siliceous shells are the fossilized skeleton of radiolarians that have been an important microplankton flourishing in marine environments since the Cambrian. Radiolarians can be classified into polycystine, phaeodaria and acantharia. The polycystine skeletons are dominated by silica, while phaeodaria skeletons are mixtures of organic matter and silica or carbonates and acantharia skeletons are composed of a special organic matter related to chitin [14–16]. Carbonate and organic matter of radiolarians can be rapidly dissolved or degraded after death. Only polycystine skeletons can settle onto the seabed and be buried and preserved as fossils, where the insoluble siliceous skeleton evolves into a siliceous shell and cytoplasm is decomposed and transformed into cavities [17].

The genetic mechanism of fillings in radiolarian siliceous shell cavities, a controversial topic, is poorly investigated at present. Micropaleontology usually uses pretreatment technology to separate radiolarian siliceous shell from rocks, which also removes fillings, e.g., calcite, pyrite and organic matter, etc., from the radiolarian siliceous shell cavity. Most

studies have focused on radiolarian fossils filled with siliceous particles in the cavity, and suggested that these particles were derived from fossilized radiolarian tissue, while calcite, pyrite and organic matter were products of diagenesis [18–20]. The siliceous particles may be a diagenetic mineral that was formed in the early diagenetic stage or even at the subsidence stage, and calcite and pyrite are metasomatic minerals associated with siliceous particles [21–23]. Schieber et al. believed that siliceous particles were diagenetic minerals, which may be formed during the early diagenetic stage or even sedimentation stage, while calcite and pyrite were metasomatic minerals of siliceous particles. Milliken et al. (2021) believed that calcite and pyrite in radiolarian siliceous shell cavities were prior to and was replaced by siliceous particles. Loucks et al. (2014) established a conceptual model of the diagenesis sequence of shale reservoirs through observing argon-ion polished samples with a scanning electron microscope [24]. They believed that radiolarian siliceous shell cavities were not filled at the early diagenetic stage, instead, they were partly filled by calcite at a later stage and were finally filled and occupied by charged oil. Lu et al. (2018) believed that siliceous particles were derived from fossilized radiolarian components and organic matter was produced by crude oil cracking. Longman et al. (2019) believed that calcite and pyrite were authigenic minerals filling dissolved space in siliceous shells. Summarily, the lack of typical and sufficient petrological evidence in these studies has brought uncertainties regarding genetic mechanisms of fillings in radiolarian siliceous shell cavities.

Taking the Upper Ordovician Wufeng–Lower Silurian Longmaxi shale in Sichuan Basin as an example, this study investigated fillings of radiolarian siliceous shell cavities through: (1) observing and characterizing the occurrence of calcite, pyrite, siliceous particles and organic matter in radiolarian siliceous shell cavities; (2) identifying the filling development sequence; (3) investigating filling generation mechanism; (4) analyzing organic pore carriers (in situ organic matter or migrated organic matter).

2. Geological Setting

Sichuan Basin is a polycyclic superimposed basin with huge hydrocarbon potential in the Yangtze Plate [25–28]. The Central Sichuan Uplift, Central Guizhou Uplift and Jiangnan-Xuefeng Uplift surrounding the basin were uplifted in the Late Ordovician, forming a deep-water shelf system with three uplifts and one sag. As a result, a low-energy, uncompensated and anoxic environment was widely formed (Figure 1), depositing radiolarian-rich black shale from the later stage of the Wufeng period to the early stage of the Longmaxi period with thickness of about 80 m. The geological setting enabled the Wufeng-Longmaxi black shale to have high gas enrichment potential [29–33].

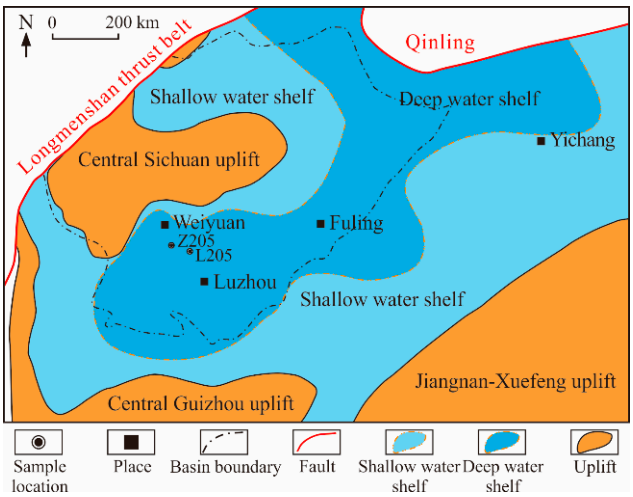

Figure 1. Sedimentary facies of Wufeng-Longmaxi shale in Sichuan Basin (modified from Wang et al., 2017 [30] and Nie et al., 2020 [31]).

The Wufeng Formation and Longmaxi Formation have generally experienced two uplift events and one subsidence event [34]. The Sichuan Basin was tectonically uplifted during the Later Silurian to the Early Permian, and the burial depths of Wufeng Formation and Longmaxi Formation were still preserved with burial depth > 500 m. The continued subsidence from the Early and Middle Permian to the early Cretaceous resulted in the maximum burial depth of Wufeng Formation and Longmaxi Formation becoming up to 6500 m, with paleotemperature over 200 °C, the maturity of organic matter in black shale reaches the over-mature stage [35,36] could form ultra-deep shale reservoirs. However, the uplift since the Late Cretaceous generally led to erosion of thickness of 1000–4000 m. As a result, the burial depth of Wufeng-Longmaxi shale is currently 3000–5500 m (Figure 2).

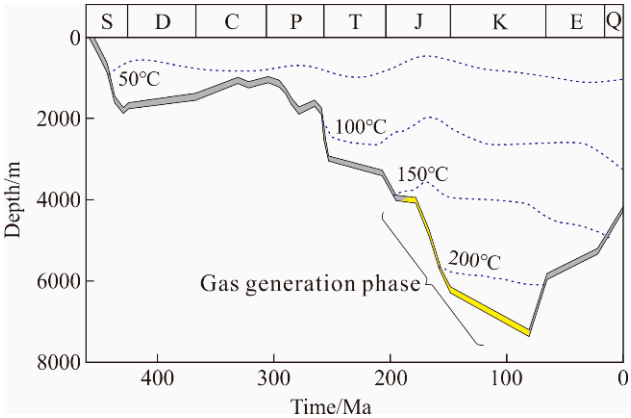

Figure 2. Burial history of Wufeng-Longmaxi shale in Sichuan Basin (modified from Guo et al., 2022 [36]).

The Wufeng-Longmaxi shale in the Sichuan Basin and its periphery is the primary shale gas producer, playing a significant role in shale gas commercial development in China, with an annual output over 200 $\times$ 10^8 m^3.

3. Methods

Typical methods, including thin section examination, X-ray diffraction, total organic carbon determination, scanning electron microscopy observation, etc., were performed on Wufeng-Longmaxi samples in this work, where X-ray diffraction and total organic carbon determination can identify mineral compositions and organic matter abundance (TOC), respectively, while thin section examination and scanning electron microscopy observation can directly exhibit the occurrence of minerals and organic matter. A large amount of mineral composition and TOC data has been acquired from the X-ray diffraction and total organic carbon determination. After that, lithofacies were classified based on thin sections and SEM images, which were dominated by radiolarian-bearing siliceous shale with TOC > 3.0%, indicating a high-quality shale reservoir [37–40].

Five Wufeng-Longmaxi radiolarian-rich siliceous shale laminae were selected from four wells as investigated samples (Figure 1 and Table 1). After siliceous shell and cavity filling observation under an optical microscope, electron probe microscopy analysis (EPMA) (platinum plating) was carried out on fillings to obtain spectral images, in situ detection data and element scanning images (Figure 3 and Table 2). Scanning electron microscope (SEM) observation was performed on gold-plated fresh samples and iridium-plated (argon-ion-polished) samples to obtain secondary electron (SE), back scattering (BSE) and energy spectrum images (Figure 4) to analyze filling occurrence and characterize the ultramicroscopic petrological features. Optical microscope observation was completed on a NIKON LV100POL microscope at the State Key Laboratory of Oil and Gas Resources and Exploration, China University of Petroleum (Beijing, China). Electron probe microscope observation and detection were performed on TXA-8230 electron equipment at the Materials Laboratory of Tsinghua University. The fresh sample observation was also completed

at the State Key Laboratory of Oil and Gas Resources and Exploration, China University of Petroleum (Beijing, China), using FEI QUANTA 200 F equipment. Argon-ion polishing and scanning electron microscope observation were completed on a FISCHIONE MODEL 1060 instrument and FEI HELIOS 650 field emission scanning electron microscope, respectively, at the National Energy Shale Gas Research and Development (Experiment) Center at Langfang Branch of PetroChina Exploration and Development Research Institute.

Table 1. Information about radiolarian-rich shale laminae.

No.	Well	Depth/m	Fm.	Thickness/mm
H202-1	Huang202	4079.03	Longmaxi	3.2
L205-1	Lu205	4031.23	Longmaxi	3.1
L207-1	Lu207	3461.58	Wufeng	1.0
Z205-1	Zi205	4103.37	Wufeng	4.8
Z205-2	Zi205	4103.96	Wufeng	1.8

An optical microscope, electron probe microscope and high-resolution scanning electron microscope can successively change magnification from ×10 to ×1000, and even to ×50,000. The observed organic–silicon complex correspondingly changes from black (Figure 3a,e), high-density bright spots on a gray background (Figure 3c,d,f,i) to high-definition images (Figure 4i–k), developing a series of evidence with resolution from low to high and view from large to small. Consequently, the interaction between calcite (>30 μm) and siliceous particles (<1 μm) can be clearly presented, providing typical petrological evidence for the occurrence of fillings with various sizes. It can lay a solid foundation for the investigation on filling genetic mechanism.

Samples were cut perpendicular to laminae that were adjusted to be horizontal during observation, where roughly ensuring samples in the underground state is helpful to understand compaction of overburden.

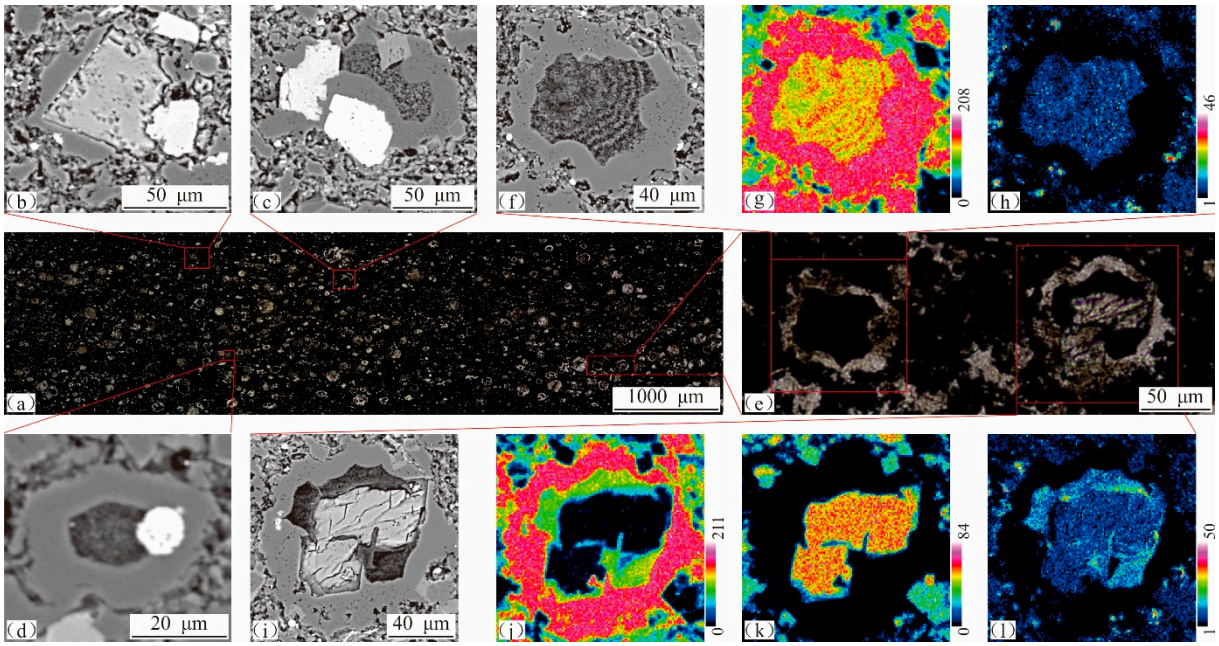

Figure 3. Typical images of fillings of radiolarian siliceous shell cavities under optical microscope and electron probe microscope. (**a**) Radiolarian-rich siliceous shale lamina with length of 6.9 mm and width of 1.8 mm. (**b**) Uncompleted radiolarian siliceous shell, cavity filled with calcite and pyrite. (**c**) Uncompleted radiolarian siliceous shell, filled with calcite, pyrite and organic–silicon complex.

(**d**) Complete radiolarian siliceous shell, filled with pyrite and organic–silicon complex. (**e**) Complete radiolarian siliceous shell, filled with calcite (white) and organic–silicon complex (black). (**f**) Spectral image of radiolarian siliceous shell on the left of image (**e**). (**g**) The scanned silicon element of image (**f**). (**h**) The scanned carbon element of image (**f**). (**i**) Spectral image of radiolarian siliceous shell on the right of image (**e**). (**j**) The scanned silicon element of image (**i**). (**k**) The scanned calcium element of image (**i**). (**l**) The scanned carbon element of image (**i**). (**a**,**e**): Plain light. (**b**–**d**,**f**,**i**): Spectral image. (**g**,**h**,**j**–**l**): Element scanning.

Table 2. In situ detected chemical compositions of calcites in radiolarian siliceous shell cavities.

No.	Well	Depth/m	Sample Location	Results/Mass/%													
				CaO	FeO	MgO	MnO	Na_2O	K_2O	Al_2O_3	SiO_2	P_2O_5	BaO	TiO_2	SrO	CO_2	Total
H202-1	Huang202	4079.03	1	55.645	0.301	0.148	0.079	0.018	0.024	0.014	0.019	0.015	0.002	/	/	43.721	99.986
			2	55.601	0.241	0.057	0.356	0.008	0.012	0.031	/	0.014	/	/	/	43.687	100.007
L205-1	Lu205	4031.23	1	55.585	0.331	0.159	0.279	/	/	/	/	0.030	/	0.002	/	43.674	100.060
			2	55.672	0.345	0.116	0.321	0.013	/	/	0.002	0.003	/	/	/	43.742	100.214
L207-1	Lu207	3461.58	1	55.929	0.040	0.021	0.019	/	0.017	0.015	0.011	0.003	/	/	/	43.942	99.997
			2	54.956	0.491	0.119	0.237	0.003	0.014	0.012	/	0.066	/	0.015	/	43.180	99.093
Z205-1	Zi205	4103.37	1	55.653	0.277	0.141	0.214	/	0.026	0.005	0.007	0.039	/	/	/	43.727	100.089
			2	55.435	0.416	0.102	0.067	/	0.005	/	/	0.024	/	/	/	43.556	99.605
Z205-2	Zi205	4103.96	1	55.872	0.080	0.013	0.028	/	0.008	0.015	0.008	0.041	/	0.005	/	43.899	99.969
			2	55.814	0.143	0.127	0.079	/	0.078	0.010	0.009	0.026	/	/	/	43.854	100.141

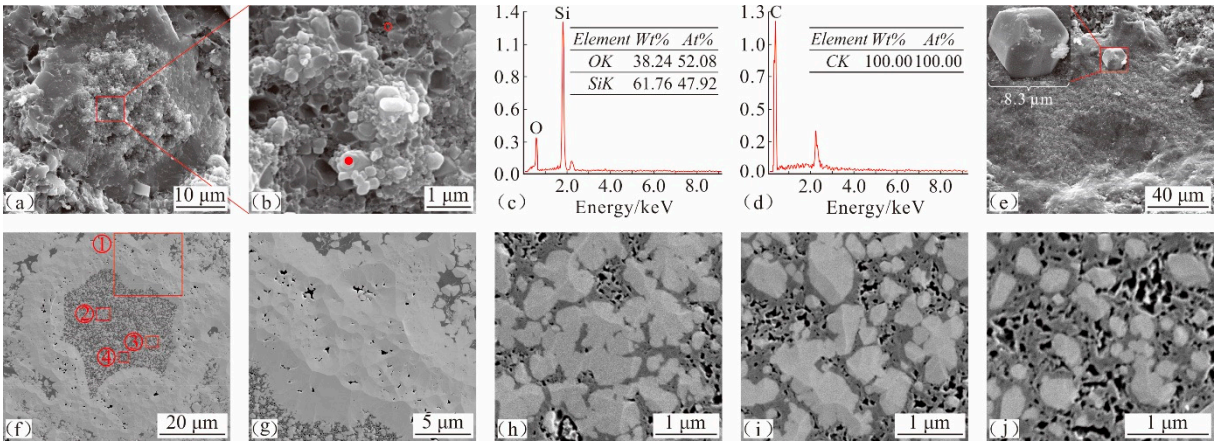

Figure 4. Typical SEM images and energy spectra of fillings in radiolarian siliceous shell cavities. (**a**) Complete radiolarian siliceous shell filled with organic–silicon complex. (**b**) Enlargement of the red box in image (**a**), organic–silicon complex. (**c**) Energy spectrum of siliceous particle in image (**b**). (**d**) Energy spectrum of organic matter in image (**b**). (**e**) Complete radiolarian siliceous shell filled with pyrite crystal. (**f**) Complete radiolarian siliceous shell filled with organic–silicon complex. (**g**) Enlargement of No. ① red box in image (**f**), pores of radiolarian siliceous skeleton. (**h**) Enlargement of No. ② red box of image (**f**), contacted silica particles with organic matter among them. (**i**) Enlargement of No. ③ red box of image (**f**), with equal silicon content and organic matter content. (**j**) Enlargement of No. ④ red box of image (**f**), scattered silica particles in organic matter. (**a**,**b**,**e**): Fresh surfaces. (**f**–**j**): Argon-ion-polished surfaces.

4. Results

4.1. Characteristics of Radiolarian Siliceous Shells

Radiolarian siliceous shells can be divided into two types, complete ones and uncompleted ones. The former have a relatively complete shell that can seal fillings in cavities (Figure 3d,e,f,i and Figure 4a,e,f). The latter have an uncompleted shell, where some fillings are in direct contact with minerals outside the shell (Figure 3b,c).

These shells are mainly round and oval in shape, with size of 50–350 μm. They can be divided into three layers from inside to outside, including the inner layer, the middle

layer and the outer layer, successively. The inner and outer layers have high density with no pores, and the middle layer has disconnected micro–nanopores (Figure 4f,g). They are about 10–100 µm in thickness, varying in the following order: middle layer > outer layer > inner layer (Figures 4g and 5a,b). The middle and outer layers are stably distributed, while the inner layer is unstable. The inner layer can be thinned or missing at the contact with calcite (Figure 5c), and can be developed at contacts with organic matter or siliceous particles (Figures 4h and 5b).

The middle layer with abundant pores is a siliceous skeleton. The skeleton of living radiolarians and other siliceous organisms is defined as opal-A in mineralogy, which is composed of colloidal SiO_2, silica and a small amount of water [41]. After radiolarian death, due to the effect of temperature and pressure, opal-A transformed to opal CT, and gradually formed cryptocrystalline with high hardness structure during the diagenetic evolution, and then transformed to quartz and finally developed into secondary silica or quartz enlargement. At the same time, a large number of micropores can be developed in siliceous skeletons [42–44] while the inner and outer layers with no pores are secondary quartz overgrowths. Additionally, microbial activities can provide a silicon source for secondary quartz overgrowths.

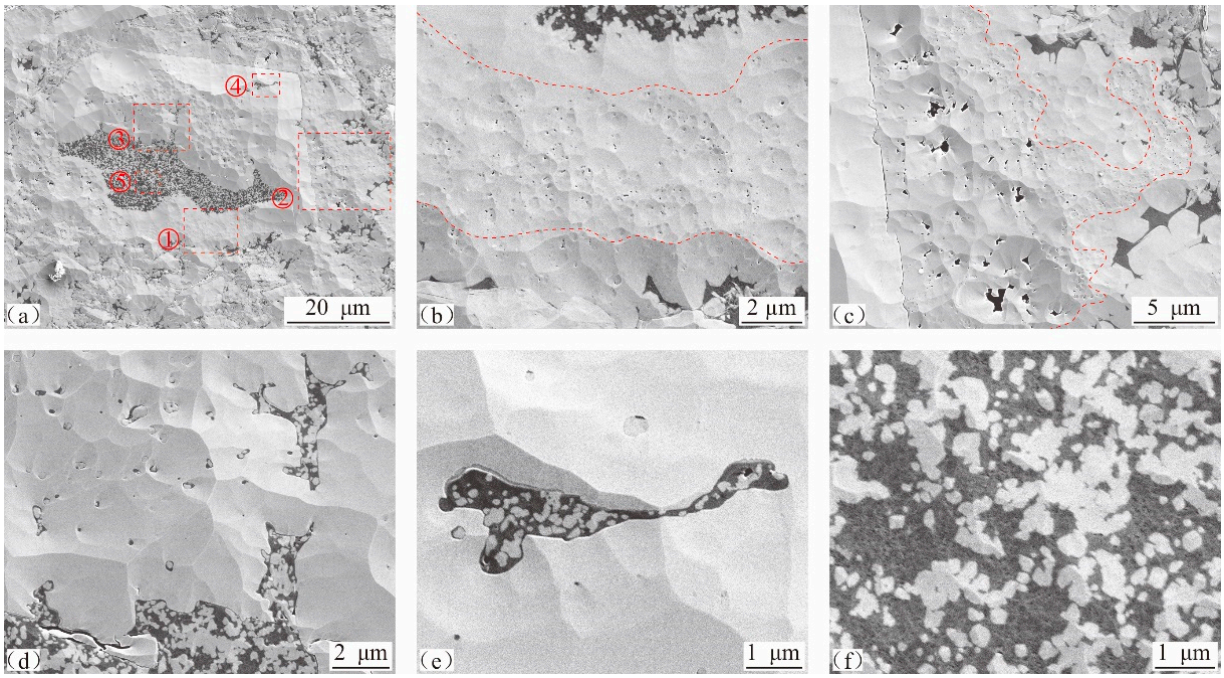

Figure 5. Typical images of uncompleted radiolarian siliceous shells with calcite and organic–silicon complex in cavities. (**a**) Uncompleted radiolarian siliceous shell cavity filled with calcite and organic–silicon complex. (**b**) Enlargement of No. ① red box in image (**a**), three layers of shell. (**c**) Enlargement of No. ② red box in image (**a**), calcite contacting with middle layer. (**d**) Enlargement of No. ③ red box, organic–silicon complex filling dissolved pores at the edge and inside of calcite. (**e**) Enlargement of No. ④ red box, organic–silicon complex filling dissolved pores within calcite. (**f**) Enlargement of No. ⑤ red box, organic–silicon complex.

4.2. Characteristics of Radiolarian Siliceous Shell Cavities

Radiolarian siliceous shell cavities can be divided into two types based on whether the shell is complete or not. A type I cavity with a complete shell is 30–250 µm in size, which is commonly filled by calcite, pyrite, siliceous particles and organic matter (Figures 3d–l and 4). A type II cavity with an uncompleted shell shares similar fillings, where fillings are in contact with minerals outside the shell (Figures 3b,c and 5a).

The calcite is straight at its contact with the cavity and the inner layer of the shell is thinned or missing (Figures 3j–l and 5c). Calcite is mostly crescent-shaped and is filled by pyrite at its contact with pyrite (Figure 3b). It is significantly dissolved and is filled by organic–silicon complex at its contact with the complex (Figures 3e,i–l, 5d and 6). Abundant dissolution pores are developed within calcite and are filled with organic–silicon complex (Figure 5d,e). Zigzags are obvious at the contact between calcite and particles outside the shell, indicating intensive dissolution (Figure 6c).

The size of siliceous particles in organic–silicon complexes is <1 μm, generally not exceeding 2 μm (Figure 4i,j). The occurrence of organic–silicon complexes can be summarized as the following. (1) The first is abundant silicon with minor organic matter. It is common for microareas or cavities to be filled only by silicon particles (Figure 4h). Siliceous particles are crowded together and related pores are filled by organic matter. (2) Organic matter and silicon are mixed evenly with similar content (Figure 4i). (3) Abundant organic matter with minor silicon. In this case, silicon particles are scattered on organic matter in a star shape (Figure 4j).

Pyrite has low content compared with calcite and organic–silicon complex, and commonly occurs as a single crystal filling a cavity alone (Figure 7a–c) or mixed with calcite (Figure 7d–f) and organic–silicon complex (Figures 3c,d and 4e).

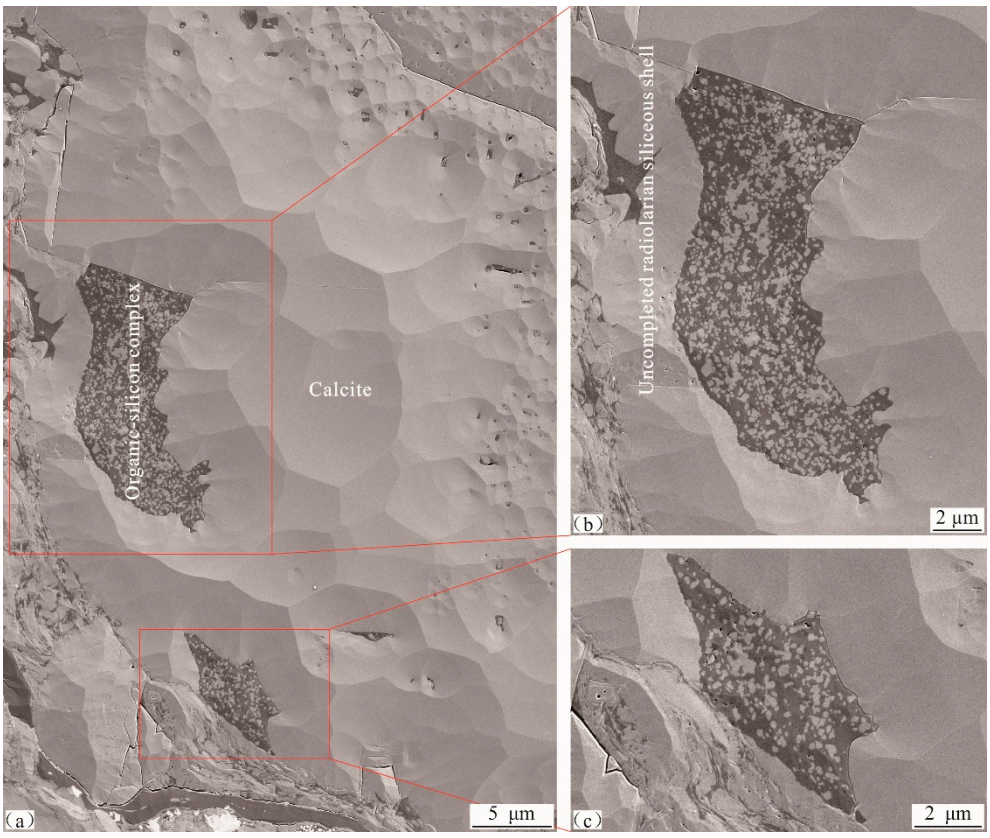

Figure 6. Typical images of calcite dissolution and organic–silicon complex in uncompleted radiolarian siliceous shell cavities. (**a**) Calcite and organic–silicon complex in the uncompleted radiolarian siliceous shell cavity. (**b**) Enlarged image (**a**), dissolved pores of calcite, filled by organic–silicon complex with no pores. (**c**) Enlarged image (**a**), no pores in organic–silicon complex contacting with clay minerals.

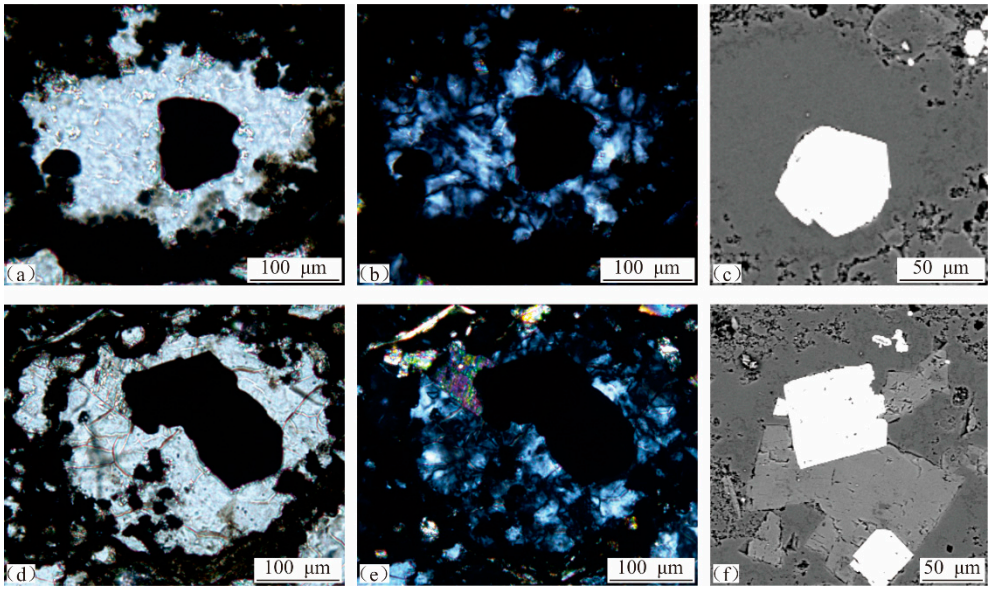

Figure 7. Typical images showing radiolarian siliceous shell cavities filled with pyrite. (**a**,**b**) Cavity filled with pyrite. (**a**). Plain light. (**b**). Perpendicular light. (**c**) Cavity filled with pyrite. (**d**,**e**) Cavity filled with pyrite, dissolved pores within calcite. (**d**). Plain light. (**e**). Perpendicular light. (**f**) Pyrite and calcite in cavity, pyrite in dissolved pores within calcite.

Nanoscale organic pores are well developed in organic–silicon complexes in type I cavities (Figure 4h–l), whereas they are not developed in type II cavities (Figures 5 and 6). This difference may be caused by their compressive strength. Shells of type I cavities can significantly protect organic pores from overburden pressure and, as a result, organic pores will not collapse and disappear. However, organic pores in type II cavities cannot be well protected by uncompleted shells, where intensive compaction can decrease or even disappear organic pores.

The impact of structure on shale gas enrichment has been discussed in the "geological setting" section, which was conducive to the black shale deposition, the thermal maturation and the shale gas preservation. This paper focuses on filling behavior in ultra-microradiolarian siliceous shell cavities as well as its origin and evolution, which is basically not directly related to the macrostructure.

5. Discussion

5.1. Filling Sequences

Organic–silicon complex occurrence suggests that organic matter and silicon particles were developed at the same period. Scattered silica particles in organic matter (Figure 4j) indicate that the development of silica particles was later than that of organic matter, otherwise these silica particles would fall to and accumulate at the bottom of the cavity under gravity. The isolated organic matter on siliceous particles (Figure 4h) suggests that organic matter could not be formed prior to the siliceous particles and, if not, organic matter would fall to the bottom under gravity as a cotton-shaped block. Therefore, only the synchronicity of organic matter and siliceous particles can reasonably explain the occurrence. In other words, the micropetrography of organic–silicon complexes does not support the assumption of oil filling pores among siliceous particles in the Wufeng-Longmaxi shale in the Sichuan Basin [45].

The organic–silicon complex of dissolved pores (Figures 3e,j–l, 5d,e and 6) at the edge and inside of calcite suggests that the calcite was developed earlier than the complex, and so was pyrite (Figure 7c,d). Pyrite is distributed in organic–silicon complexes (Figures 3c,d and 4e), indicating that pyrite was developed prior to the organic–silicon complex. The petrology evidences that pyrite metasomatism organic–silicon complex [46] cannot occur in Wufeng-Longmaxi shale in the Sichuan Basin. Firstly, pyrite has a crystal shape with a smooth surface and straight edges (Figure 4e,f). Secondly, siliceous particles with stable chemical properties are insoluble in both acidic and alkaline fluids. However, where did these mysterious fluids come from? Thirdly, although organic matter has inactive chemical properties, what was the origin of the mysterious fluid congruently dissolving organic matter? Finally, where did Fe^{2+} and S^{-} come from?

The occurrence and interaction of fillings in cavities suggest that the filling sequence in the Wufeng-Longmaxi shale in Sichuan Basin is calcite, pyrite, organic–silicon complex. Calcite dissolution provided space for pyrite or organic–silicon complex, hence, cavities might be fully filled by pyrite or organic–complex when calcite is completely dissolved, while it might be filled by residual calcite and pyrite or organic–silicon complex when calcite is partially dissolved.

5.2. Filling Development Period

Full filling of type II cavities by calcite, pyrite and organic–silicon complex suggests that fillings were formed before the radiolarian siliceous shells fell to the water–sediment interface. The residual siliceous shells would not be in a round or oval pattern if calcite was formed above or below the interface, instead, they would be cracked into scattered fragments under gravity. Clay minerals and pyrite framboids might fill dissolved pores associated with calcite [47–50] when organic–silicon complex was formed above or below the interface, where residual shells may be cracked into fragments under gravity. However, these phenomena have not been found in the Wufeng-Longmaxi shale in Sichuan Basin. Therefore, fillings were formed before the radiolarian siliceous shells were deposited onto the water–sediment interface.

Radiolaria are plankton living at the ocean surface, and their organic component can be decomposed rapidly after death [51]. The insoluble siliceous skeleton can be developed into a siliceous shell, and cytoplasm in the cyst can be decomposed into a cavity. Calcite filling, calcite dissolution, pyrite precipitation and organic–silicon complex filling can occur successively in cavities during siliceous shell settlement. Meanwhile, shells may be broken into fragments by wave action or collisions among each other, and then be preserved under cementation.

Summarily, the micropetrography of fillings of the Wufeng-Longmaxi shale in Sichuan Basin obviously does not support the assumption that calcite was formed at the diagenesis stage.

5.3. Calcite Development Process

Calcite in black shale can be sourced from terrigenous detritus, chemical precipitation [52] and authigenic calcite during diagenesis [53,54]. Calcite in radiolarian siliceous shell cavities of Wufeng-Longmaxi shale samples in Sichuan Basin was formed before burial, which could not be produced by diagenesis. Terrestrial calcite fragments experiencing physical and chemical weathering after long-distance transportation commonly have an irregular surface and shape. The contact between calcite and the cavity wall does not support that. Furthermore, it is impossible for such a large number of terrigenous fragments with such a large size to enter these closed shells, also indicating that they could not be derived from terrigenous input. Therefore, the seawater chemical precipitation is the only calcite source.

Precipitated calcite on the water surface is typically produced by biological activities, some of which is a secreted by-product of photosynthesis [55]. Shallow sea water (<100 m, especially the 10 m at the top) and sufficient light near the equator enable biological photosynthesis to produce sufficient calcite, which is commonly suspended in the water

body as flocculent particles. It is defined as a carbonate factory with high productivity. The Sichuan Basin was located near the equator during the Late Ordovician to Early Silurian [56], where radiolarians and microorganisms producing carbonate flourished on the seawater surface. They could produce abundant flocculated calcite particles, filling radiolarian siliceous shell cavities in a short time.

The weight of cavities filled with calcite increases settlement speed and shortens time from seawater surface to seabed, which is conducive to preservation. However, the most significant variation during calcite settlement is dissolution, where carbonate compensation depth (CCD), carbonate lysocline depth (CLD) and carbonate saturation depth (CSD) are three important interfaces [57–60]. Calcium carbonate is saturated in shallow sea water and becomes unsaturated in the deep part because its solubility increases with decreasing temperature and increasing pressure. The CSD is a turning point that alters calcium carbonate from saturated to unsaturated and dissolves calcite significantly. The calcite is weakly dissolved above CLD and is largely dissolved below CLD. The CCD can be regarded as a snow line on land, where sediments in the shallow zone are rich in calcite and sediments in the deep zone are poor in calcite. Water depth with calcite content of 10% is used to define the line in practice. The CSD, CLD and CCD not only differ among oceans, but also vary greatly within the same ocean. The CSDs of the North Atlantic, the South Atlantic, the northern Pacific and offshore Peru are 4000 m, <2500 m at the shallowest point, within 500 m and below surface water, respectively. The average CCDs of the Pacific Ocean, Indian Ocean and Atlantic Ocean are 4500 m, 5000 m and 5300 m, respectively. Generally, the CSD is usually several hundred meters above the CCD. The CCD gradually deepened in the Phanerozoic, from hundreds of meters to thousands of meters in the Early Paleozoic to 4000 m below at present [61]. The average calcite content of the Wufeng-Longmaxi shale in Sichuan Basin is <10% [62,63]. It can be inferred that the shelf during the Late Ordovician to Early Silurian was generally below the CCD, where calcite developing at the sea surface was intensively dissolved after CSD, CLD and CCD, and only a small portion of calcite settled and was preserved on the seabed. Hence, calcite observed in radiolarian siliceous shell cavities is the residual type that was not fully dissolved.

5.4. Pyrite Development Process

Pyrite in sediments is closely related to thermochemical sulfate reduction (TSR) under high temperature (100–140 °C) in deep basins and bacterial sulfate reduction (BSR) near the water–sediment interface [64]. Pyrite particles in radiolarian siliceous shell cavities of the Wufeng-Longmaxi shale in Sichuan Basin were formed above the water–sediment interface, which were independent of TSR. BSR is usually involved in pyrite framboid growth. The environment, e.g., anoxic water body containing dissolved hydrogen sulfide, interface between oxygenated water and organic-rich sediment as well as below, etc., is favorable for the development of pyrite framboids [47,65]. Currently, the origin of pyrite framboids in sediments is being widely investigated, while pyrite particles are poorly understood [66–68].

Particle size statistics suggest that pyrite framboids from the Wufeng-Longmaxi shale in Sichuan Basin were developed in an anoxic water body, where BSR near the water–sediment interface provided hydrogen sulfide to reduce terrestrial Fe^{3+} into Fe^{2+}, resulting in pyrite precipitation. Hence, pyrite particles in cavities should be precipitated above the anoxic water body, i.e., the oxygenated water body. Li et al. (2009a, 2009b) [69,70] found that pyrite particles were developed within shell cavities associated with Tasmanite algae in siliceous limestone and foraminifera in marl, but were not developed outside shells. They held that although high oxygen content in a sedimentary environment was negative for pyrite precipitation, biological cavities provided a relatively anoxic environment for pyrite precipitation. Similarly, pyrite particles can fill radiolarian siliceous shell cavities.

Calcite dissolution occurs to generate dissolved pores and form a closed and anoxic environment when cavities filled with calcite settle below the CSD. It can promote sulfate reducing bacterial growth and provide an excellent environment for pyrite precipitation.

An anoxic environment may delay oxidation decomposition of dissolved hydrogen sulfide, also contributing to pyrite precipitation.

5.5. Organic–Silicon Complex Development Process

Four origins of authigenic silica in black shale reservoirs have been identified by previous studies, including biological silica dissolution, microorganisms producing silica, smectite–illite transformation and pressure dissolution of siliceous minerals. Clay mineral transformation and pressure dissolution commonly occur during diagenesis, which are not a silica source for radiolarian siliceous shell cavities. The biological silica dissolution can be divided into two stages. The first stage involves the dissolution of exposed siliceous skeletons in sea water after organism death [71]. Fifty to sixty percent of biological opal precipitating in surface sea water can be dissolved within a water depth < 100 m [72], where dissolution rate is positively correlated with seawater temperature [73,74]. The second stage is the biological opal transforming into quartz and releasing silica into fluid during the early diagenetic stage, which can provide a source for authigenic quartz enlargement or secondary quartz enlargement. Obviously, the radiolarian fillings were formed before the radiolarian siliceous shells fell to the water–sediment interface. The biological silica dissolution in the second stage cannot provide a silica source for the radiolarian siliceous shell cavities. Actual geological data suggest that quartz secondary enlargement is more obvious than biological silica dissolution at the Wufeng-Longmaxi shale, indicating that the first stage is also not a primary silica source. Therefore, the microorganisms producing silica are the main source for siliceous particles in cavities of the Wufeng-Longmaxi shale in Sichuan Basin. The microbial origin of authigenic siliceous particles in shale reservoirs has been gradually accepted [75].

Organic matter in the ocean can be divided into dissolved organic matter (DOM) and particulate organic matter (POM) based on particle size, while the DOM can be subdivided into colloidal organic matter (COM) and low-molecular-weight dissolved organic matter (LMW DOM). The DOM is the largest organic carbon pool in the ocean, accounting for about 90% of the organic carbon [76,77]. DOM is characterized by stable property, difficult decomposition, high molecular weight and complex structure derived from biomineralization and debris under chemical and biochemical processes. Typical chemical activities, e.g., solubility, ionization, colloid and large specific surface area [78–80] enable it to combine with terrigenous clay minerals with similar chemical activity to form organic–clay mineral complex [81–83]. However, no organic–clay mineral complex was found in radiolarian siliceous shell cavities from the Upper Ordovician to Lower Silurian in Sichuan Basin, indicating that DOM was not the organic matter source. Based on silica source analysis above, it is believed that microorganisms producing silica may be the main organic matter source.

The calcite dissolution can be accelerated when radiolarian siliceous shells filled with calcite and minor pyrite subside below the CLD, which provides favorable space for microorganism growth. In this case, microbes thrive with active metabolism promoting organic–silicon complexes to rapidly fill dissolved pores. It occurs in an anoxic environment, contributing to the preservation of organic–silicon complex. Organic–silicon complex isolates calcite or hinders the contact between calcite and sea water, and further inhibits calcite dissolution, creating a favorable environment for infilling of calcite, pyrite and organic–silicon complex. However, the microorganisms producing silicon are poorly understood, and require more future work, especially detailed investigation on radiolarian siliceous ooze deposited in modern oceans.

Radiolarian siliceous shells can be preserved as laminae in the seabed after deposition. Organic matter can be transformed into kerogen with increasing burial depth and formation temperature, which is then thermally degraded into hydrocarbon and bitumen [84,85]. Overpressure derived from hydrocarbon generation can discharge oil and gas from cavities, where honeycomb-like pores appear in the organic–silicon complex. The remaining gas in pores is part of the shale gas. Different from that, the organic–silicon complex in uncom-

pleted cavities has no organic pore growth, which is caused by mechanical compaction. The complete radiolarian siliceous shell can protect organic pores in cavities from overburden pressure, however, an uncompleted shell has limited capacity to withstand the pressure, where intense compaction can collapse and even disappear organic pores. Therefore, the organic pore carrier is a weakly compacted organic matter.

Two conflicting views are currently presented about organic pore carriers in shale reservoirs: sedimentary organic matter and migrated organic matter. Research performed by Loucks and his team, the pioneer in studying organic pore origin through conducting micropetrography on shale samples with argon-ion-polishing technology, exhibits difficulties in investigating the configuration between organic pores and organic matter type. Specifically, initial research showed that organic pores were primarily developed in sedimentary organic matter [86–88]. After that, they reported that honeycomb-like organic pores were mainly developed in migrated organic matter. Recently, they emphasized that appropriate solutions and technologies were required to understand organic pore carriers [88]. The lack of typical petrological evidence that directly reflects the sedimentary and diagenetic processes of shale and the thermal evolution of organic matter is the root cause of the polysolubility of organic pore carriers. Our investigation suggests that the only way to elucidate organic pore carriers and understand sequences and development processes of minerals and organic matter is to select weakly compacted radiolarian siliceous shale laminae to carry out micro- and ultra-micropetrological observation and geochemical testing via various technologies.

6. Conclusions

The development sequence and material source of various fillings are investigated via ultra-micropetrology observation of filling types and occurrence in radiolarian siliceous shell cavities and their relationship with other minerals and organic matter. After that, the formation and preservation mechanism of honeycomb-like pores in organic matter were discussed. The conclusions can be summarized as the following:

(1) Both complete and uncompleted radiolarian siliceous shells were abundant in Wufeng-Longmaxi radiolarian siliceous shale laminae in Sichuan Basin, which was filled with calcite, pyrite and organic–silicon complex.

(2) Fillings in radiolarian siliceous shell cavities were developed in the following order: calcite, pyrite, organic–silicon complex. Calcite was developed during sedimentation of radiolarian siliceous shells, after that pyrite and organic–silicon complex successively filled dissolved pores associated with calcite.

(3) Calcite was derived from microbial activities producing calcium carbonate at the seawater surface. The radiolarian siliceous shell cavity promotes sulfate reducing bacterial growth or dissolved hydrogen sulfide reducing Fe^{3+} into Fe^{2+}, contributing positively to pyrite development. The organic–silicon complex was produced by the metabolism of microorganisms.

(4) Complete radiolarian siliceous shells could withstand overburden pressure, where honeycomb-like organic pores were developed in organic–silicon complex. However, uncompleted radiolarian siliceous shells had weak compressive strength and, as a result, organic pores were poorly developed in organic–silicon complex.

(5) The only approach to figure out organic pore carriers and investigate sequences and development processes of minerals and organic matter is to select weakly compacted radiolarian siliceous shale laminae to carry out micro- and ultra-micropetrological observation and geochemical testing on weakly compacted radiolarian siliceous shale laminae.

Author Contributions: Methodology, X.L.; investigation, J.Y.; resources, X.Z. (Xiaowei Zhang); writing—original draft preparation, X.Z. (Xiaofeng Zhou) and P.L.; writing—review and editing, W.G. All authors have read and agreed to the published version of the manuscript.

Funding: This research was funded by the 14th Five-Year Plan of the Ministry of Science and Technology of PetroChina, grant number: 2021DJ1901. And the APC was funded by China University of Petroleum.

Data Availability Statement: All data generated or used during the study appear in the submitted article.

Conflicts of Interest: The authors declare no conflict of interest.

References

1. Turgeon, S.; Brumsack, H.J. Anoxic vs dysoxic events reflected in sediment geochemistry during the Cenomanian-Turonian Boundary Event(Cretaceous)in the Umbria-Marche Basin of central Italy. *Chem. Geol.* **2006**, *234*, 321–339. [CrossRef]
2. Ross, D.J.; Bustin, R.M. Sediment geochemistry of the Lower Jurassic Gordon dale Member, northeastern British Columbia. *Bull. Can. Pet. Geol.* **2006**, *54*, 337–365. [CrossRef]
3. Ross, D.J.; Bustin, R.M. Investigating the use of sedimentary geochemical proxies for paleo environment interpretation of thermally mature organic-rich strata: Examples from the Devonian-Mississippian shales, Western Canadian Sedimentary Basin. *Chem. Geol.* **2009**, *260*, 1–19. [CrossRef]
4. Du, Y.D.; Shen, J.; Feng, Q.L. Applications of radiolarian for productivity and hydrocarbon-source rocks. *Earth Sci. J. China Univ. Geosci.* **2012**, *37*, 147–155.
5. Wang, S.; Zou, C.; Dong, D.; Wang, Y.; Huang, J.; Guo, Z. Biogenic silica of organic-rich shale in Sichuan basin and its significance for shale gas. *Acta Sci. Nat. Univ. Pekin.* **2014**, *50*, 476–486.
6. Liu, J.; Li, Y.; Zhang, Y.; Liu, S.; Cai, Y. Evidences of biogenic silica of Wufeng-Longmaxi Formation shale in Jiaoshiba area and its geological significance. *J. China Univ. Pet. Ed. Nat. Sci.* **2017**, *41*, 34–41.
7. Cao, T.T.; Deng, M.; Song, Z.G.; Liu, G.X.; Huang, Y.R.; Hursthouse, A.S. Study on the effect of pyrite on the accumulation of shale oil and gas. *Nat. Gas Geosci.* **2018**, *29*, 404–414.
8. Milliken, K.L.; Zhang, T.; Chen, J.; Ni, Y. Mineral diagenetic control of expulsion efficiency in organic-rich mudrocks, Bakken Formation (Devonian-Mississippian), Williston Basin, North Dakota, USA. *Mar. Pet. Geol.* **2021**, *127*, 104869. [CrossRef]
9. Longfei, L.U.; Jianzhong, Q.I.; Baojian, S.H.; Weixin, L.; Qingzhen, Z. Biogenic origin and hydrocarbon significance of siliceous shale from the Wufeng-Longmaxi formations in Fuling area, southeastern Sichuan Basin. *Pet. Geol. Exp.* **2016**, *38*, 460–465.
10. Lu, L.; Qin, J.; Shen, B.; Tenger. The origin of biogenic silica in siliceous shale from Wufeng-Longmaxi formation in the Middle and Upper Yangtze region and its relationship with shale gas enrichment. *Earth Sci. Front.* **2018**, *25*, 226–236.
11. Longman, M.W.; Drake, W.R.; Milliken, K.L.; Olson, T.M. *A Comparison of Silica Diagenesis in the Devonian Woodford Shale (Central Basin Platform, West Texas) and Cretaceous Mowry Shale (Powder River Basin, Wyoming)*; GeoScienceWorld: Tysons Corner, VA, USA, 2019; pp. 49–67.
12. Zhou, X.; Guo, W.; Li, X.; Xiaowei, Z.; Pingping, L.; Junmin, Y. Occurrence characteristics, genesis and petroleum geological significance of micro-nano silica-organic matter aggregate in radiolarian siliceous shell cavity: A case study of Wufeng-Longmaxi Formationin Sichuan Basin, SW China. *J. China Univ. Petrol.* **2021**, *45*, 68–79.
13. Zhou, X.; Li, X.; Guo, W.; Liang, P.; Yu, J. Characteristics, formation mechanism and influence on physical properties of carbonate minerals in shale reservoir of Wufeng-Longmaxi formations, Sichuan Basin. *Nat. Gas Geosci.* **2022**, *33*, 775–788. [CrossRef]
14. Zhang, L.L.; Chen, M.H.; Xiang, R. Progress and prospect in research on living radiolaria ecoloy: A basic study of paleoenvironmental and paleoeanographic reconstructions. *Adv. Earth Sci.* **2006**, *21*, 474–481. [CrossRef]
15. Zhang, L.L.; Chen, M.H.; Hu, W.F.; Zhang, Q.; Xiang, R. Vertical distribution of living radiolarians and its environmental implication. *J. Trop. Oceanogr.* **2013**, *32*, 101–107.
16. Zhang, J.; Zhang, L.L.; Chen, M.H.; Suzuki, N.; Qiu, Z.Y.; Cheng, X.W.; Zhang, Q. The higher level classification of modern radiolarians and their ecological significance. *Acta Micropalaeontol. Sin.* **2020**, *37*, 82–98.
17. Qiu, Z.; Zhang, L.; Hu, B.; Chang, H.; Cheng, X.; Xiang, R. Radiolarian distribution in surface sediments of the Philippine Sea and adjacent areas and its response to environment. *Mar. Geol. Quat. Geol.* **2021**, *41*, 87–101.
18. Tan, Z. A new method for the production of radiolarian skeleton specimens. *Ocean. Limnol.* **1964**, *6*, 309–310.
19. Cao, W.; Feng, Q. Treatment and separation methods of radiolarians in limestone. *Acta Micropalaeontol. Sin.* **2012**, *29*, 416–419.
20. Ma, Q.; Feng, Q.; Cao, W.; Zhang, L.; Ye, Y.; Gu, S. Radiolarian fauna from the Chiungchussuan Shuijingtuo Formation (Cambrian Series 2) in Western Hubei Province, South China. *Sci. China Earth Sci.* **2019**, *49*, 1357–1371. [CrossRef]
21. Iijima, A.; Tada, R. Silica diagenesis of Neogene diatomaceous and volcaniclastic sediments in northern Japan. *Sedimentology* **1981**, *28*, 185–200. [CrossRef]
22. Laschet, C. On the origin of cherts. *Facies* **1984**, *10*, 257–289. [CrossRef]
23. Schieber, J.; Shao, X. Detecting detrital carbonate in shale successions-Relevance for evaluation of depositional setting and sequence stratigraphic interpretation. *Mar. Pet. Geol.* **2021**, *130*, 105130. [CrossRef]
24. Loucks, R.G.; Reed, R.M. Scanning-electron-microscope petrographic Evidence for distinguishing organic-matter pores associated with depositional organic matter versus migrated organic matter in mudrocks. *Gulf Coast Assoc. Geol. Soc. J.* **2014**, *3*, 51–60.
25. Liu, S.; Zeng, X.; Huang, W.; Ma, W.-X. Basic characteristics of shale and continuous-discontinuous transition gas reservoirs in SichuanBasin, China. *J. Chengdu Univ. Technol. Sci. Technol. Ed.* **2009**, *36*, 578–592.

26. Wei, L.S.; Jinxi, Z.Y.; Lei, J. Sichuan Basin: A superimposed sedimentary basin mainly controlled by its peripheric tectonics. *Chin. J. Geol.* **2018**, *53*, 308–326.
27. Guowei, H.D.; Renqi, Z.L.; Zhu, W. Formation and evolution of multi-cycle superposed Sichuan Basin, China. *Chin. J. Geol.* **2011**, *46*, 589–606.
28. Zhili, L.U.; Jianhui, H.A.; Chao, L.U.; Qihou, L.U.; Keyou, H. The discovery, characteristics and prospects of commercial oil and gas layers/reservoirs in Sichuan Basin. *Xinjiang Pet. Geol.* **2013**, *34*, 504–514.
29. Mou, C.; Wang, X.; Wang, Q.; Zhou, K.K.; Liang, W.; Ge, X.Y.; Chen, X.W. Relationship between sedimentary facies and shale gas geological conditions of the Lower Silurian Longmaxi Formation in southern Sichuan Basin and its adjacent areas. *J. Palaeogeogr.* **2016**, *18*, 457–472.
30. Wang, Y.; Li, X.; Dong, D.; Zhang, C.; Wang, S. Main factors controlling the sedimentation of high-quality shale in Wufeng–Longmaxi Fm, Upper Yangtze region. *Nat. Gas Ind.* **2017**, *37*, 9–20. [CrossRef]
31. Nie, H.; He, Z.; Liu, G.; Du, W.; Wang, R.; Zhang, G. Genetic mechanism of high-quality shale gas reservoirs in the Wufeng–Longmaxi Fms in the Sichuan Basin. *Nat. Gas Ind.* **2020**, *40*, 31–41.
32. Shi, Z.; Zhou, T.; Guo, W.; Liang, P.; Cheng, F. Quantitative paleogeographic mapping and sedimentary microfacies division in a deep-water marine shale shel: Case study of Wufeng-Longmaxi shale, southern Sichuan Basin, China. *Acta Sedimentol. Sin.* **2022**, 1–22.
33. Xue, Y.; Xuewen, S.; Yiqing, Z.; Jia, L.; Yi, L.; Liang, H.; Liang, X.; Yanyou, L.; Yao, C.; Jiayu, J. Sedimentary evolution and organic matter enrichment of Katian-Aeronian deep-water shale in Luzhou area, southern Sichuan Basin. *Acta Pet. Sin.* **2022**, *43*, 469–482.
34. Shu-gen, L.; Bin, D.; Yong, Z. Unique geological features of burial and superimposition of the Lower Paleozoic shale gas across the Sichuan Basin and its periphery. *Earth Sci. Front.* **2016**, *23*, 11–28.
35. Wang, Y.; Qiu, N.; Yang, Y.; Rui, X. Thermal maturity of Wufeng-Longmaxi shale in Sichuan Basin. *Earth Sci.* **2019**, *44*, 953–971.
36. Guo, X.; Zhao, Y.; Shen, B.; Wei, F.; Lu, L.; Pan, A. Marine shale gas exploration theory in southern China: Review and prospects. *Acta Geol. Sin.* **2022**, *96*, 172–182.
37. Wang, X.; Mou, C.; Ge, X.; Chen, X.; Zhou, K.; Wang, Q.; Liang, W.; Chen, C. Study on clay minerals in the lower silurian Longmaxi Formation in southern Sichuan Basin and its periphery. *Nat. Gas Geosci.* **2014**, *25*, 1781–1794.
38. Ran, B.; Liu, S.; Sun, W.; Ye, Y.; Qiu, J.; Zhang, J. Lithofacies classification of shales of the Lower Paleozoic Wufeng-Longmaxi Formations in the Sichuan Basin and its surrounding areas, China. *Earth Sci. Front.* **2016**, *23*, 96–107.
39. Yu-Man, W.A.; Chu-Fang, W.A.; Da-Zhong, D.O. Lithofacies characterization of Longmaxi Formation of the Lower Silurian, southern Sichuan. *Earth Sci. Front.* **2016**, *23*, 119–133.
40. Sun, C.; Nie, H.; Liu, G.; Zhang, R.; Du, W.; Wang, R. Quartz type and its control on shale gas enrichment and production: A case study of the Wufeng-Longmaxi Formations in the Sichuan Basin and its surrounding areas, China. *Earth Sci.* **2019**, *44*, 3692–3704.
41. Qin, Y. Research progress in Early diagenesis of biogenic silica. *Geol. Rev.* **2010**, *56*, 89–98.
42. Yang, D.F.; Wei, C.D.; Ning, W.K.; Xu, S.N.; Jiang, Y.S. Structure and adsorption properties of Nenjiang opal shale. *J. Jilin Univ. Earth Sci. Ed.* **2010**, *40*, 1061–1065.
43. Chen, H.; Lu, L.; Liu, W.; Shen, B.; Yu, L.; Yang, Y. Pore network changes in opaline siliceous shale during diagenesis. *Pet. Geol. Exp.* **2017**, *39*, 341–347.
44. Lu, L.; Liu, W.; Yu, L.; Zhang, W.; Shen, B.; Teng, G. Early diagenesis characteristics of biogenic opal and its influence on porosity and pore network evolution of siliceous shale. *Pet. Geol. Exp.* **2020**, *42*, 363–370.
45. Milliken, K.L.; Olson, T. Silica diagenesis, porosity evolution, and mechanical behavior in siliceous mudstones, Mowry Shale (Cretaceous),Rocky Mountains, U.S.A. *J. Sediment. Res.* **2017**, *87*, 366–387. [CrossRef]
46. Schicker, A.; Gier, S.; Schieber, J.; Krois, P. Diagenesis of the Malmian Mikulov Formation source rock, Vienna Basin: Focus on matrix and pores. *Mar. Pet. Geol.* **2021**, *129*, 105082. [CrossRef]
47. Han, S.; Li, W. Study on the genesis of pyrite in the Longmaxi Formation shale in the Upper Yangtze Area. *Nat. Gas Geosci.* **2019**, *30*, 1–10.
48. Duan, X.; Xian, Y.; Yuan, B.; Dai, X.; Cao, J.; Liu, Z.; Liu, X. Formation mechanism and formation environment of framboidal pyrite in Wufeng Formation-Longmaxi Formation shale and its influence on shale reservoir in the southeastern Chongqing, China. *J. Chengdu Univ. Technol. Sci. Technol. Ed.* **2020**, *47*, 514–521.
49. Zhang, G.; Nie, H.; Tang, X.; DU, W.; Sun, C.; Chen, S. Pyrite type and its effect on shale gas accumulation: A case study of Wufeng-Longmaxi shale in Sichuan Basin and its periphery. *Pet. Geol. Exp.* **2020**, *42*, 459–466.
50. Grill, E.V.; Richards, F.A. Nutrient regeneration from phytoplankton decomposing in sea water. *J. Mar. Res.* **1964**, *22*, 51–69.
51. Yan, J.X.; Meng, Q.; Wang, X.; Liu, Z.C.; Huang, H.; Chen, F.Y.; Guo, Q.D. Carbonate factory and carbonate platform: Progress and prospects. *J. Palaeogeogr. Chin. Ed.* **2019**, *21*, 232–253.
52. Curtis, C.D. Diagenetic alteration in black shales. *J. Geol. Soc.* **1980**, *137*, 189–194. [CrossRef]
53. Guo, Q.; Jin, Z.; Zhao, J.; Cui, X.; Wang, J. Origin of carbonate minerals in organic matter-rich shale of Longmaxi formation in the Sichuan Basin. *Sci. Technol. Eng.* **2019**, *19*, 79–85.
54. Robbins, L.; Tao, Y.; Evans, C. Temporal and spatial distribution of whitings on Great Bahama Bank and a new lime budget. *Geology* **1997**, *25*, 947–950. [CrossRef]
55. Wu, H.; Chang, C.; Liu, C.; Zhong, D. Evolution of the Qinling Fold Belt and the movement of the north and south China blocks: The evidence of geology and paleomagnetism. *Sci. Geol. Sin.* **1990**, *25*, 201–214.

56. Zheng, L.; Chen, R. Planktonic foraminifera and deep sea carbonate dissolution. *Offshore Oil* **1982**, *1*, 41–49.
57. Wang, Y. Deep—sea carbonate compensation depth and lysocline. *Mar. Geol. Quat. Geol.* **1987**, *7*, 113–120.
58. Han, W.; Kemei, M.A. Carbonate compensation depth, saturation horizon and lysocline in the northeast region of South China Sea. *Trop. Oceanol.* **1988**, *7*, 84–89.
59. Mao, S. Ocean drilling program and the development of paleoceanography. *Geol. Sci. Technol. Inf.* **1994**, *13*, 45–52.
60. Wang, P. Geological evolution of the ocean carbon cycle. *Adv. Nat. Sci.* **2006**, *16*, 1361–1370.
61. Wang, X.; Mou, C.; Wang, Q.; Ge, X.; Chen, X.; Zhou, K.; Liang, W. Diagenesis of black shale in Longmaxi Formation, southern Sichuan Basin and its periphery. *Acta Pet. Sin.* **2015**, *36*, 1035–1047.
62. Cai, J. Study of shale reservoir diagenesis of the Wufeng—Longmaxi Formations in the Jiaoshiba area, Sichuan Basin. *J. Miner. Pet.* **2017**, *37*, 103–109.
63. Machel, H.G. Bacterial and thermochemical sulfate reduction in diagenetic settings—Old and new insights. *Sediment. Geol.* **2001**, *140*, 143–175. [CrossRef]
64. Wilkin, R.T.; Barnes, H.L.; Brantlsy, S.L. The size distribution of framboidal pyrite in modern sediments: An indicator of redox conditions. *Geochim. Cosmochim. Acta* **1996**, *60*, 3897–3912. [CrossRef]
65. Yang, X.; Gong, Y. Pyrite Framboid: Indicator of Environments and Life. *Earth Sci. J. China Univ. Geosci.* **2011**, *36*, 643–658.
66. Hu, Y.; Wang, W.; Zhou, C. Morphologic and Isotopic Characteristics of Sedimentary Pyrite: A case study from deepwater facies, Ediacaran Lantian Formation in South China. *Acta Sedimentol. Sin.* **2020**, *38*, 138–149.
67. Jiang, K.; Zhou, W.; Deng, N.; Zhang, H.; Xu, H.; Zhao, X.; Yi, T.; Yang, P. Characteristics and geological significance of pyrites in Wufeng and Longmaxi Formation reservoir shale in Sichuan Basin, China. *J. Chengdu Univ. Technol. Sci. Technol. Ed.* **2020**, *47*, 50–64.
68. Li, H.; Lu, X.; Bian, L. Formation mechanism and geological significance of the pyrite framboids in the cyst of Tasmanites in the Dalong formatin cropped in the Kuangshanliang area, Northern Sichuan Province. *Prog. Nat. Sci.* **2009**, *19*, 1082–1089.
69. Li, H.; Lu, X.; Bian, L. Formation of pyrite framboids in the chamber of foraminiferas and its geological significance: A case study of the foraminiferas fossils in the Qixia Formation in the Yanmenkou Area, Hubei Province. *Geol. J. China Univ.* **2009**, *15*, 470–476.
70. Nelson, D.M.; Goering, J.J. Near-surface silica dissolution in the upwelling region off Northwest Africa. *Deep Sea Res.* **1977**, *24*, 65–73. [CrossRef]
71. Nelson, D.M.; Tréguer, P.; Brzezinski, M.A.; Leynaert, A.; Quéguiner, B. Production and dissolution of biogenic silica in the ocean: Revised global estimates, comparison with regional data and relationship to biogenic sedimentation. *Glob. Biogeochem. Cycle* **1995**, *9*, 359–372. [CrossRef]
72. Lawson, D.S.; Hurd, D.C.; Pankratz, H.S. Silica dissolution rates of decomposing phytoplankton assemblages at various temperatures. *Am. J. Sci.* **1978**, *278*, 1–22. [CrossRef]
73. Kamatani, A. Dissolution rates of silica from diatoms decomposing at various temperatures. *Mar. Biol.* **1982**, *68*, 91–96. [CrossRef]
74. Stolper, D.A.; Love, G.D.; Bates, S.; Lyons, T.W.; Young, E.; Sessions, A.L.; Grotzinger, J.P. Paleoecology and paleoceanography of the Athel silicilyte, Ediacaran-Cambrian boundary, Sultanate of Oman. *Geobiology* **2017**, *15*, 401–426. [CrossRef] [PubMed]
75. Hedges, J.I.; Keil, R.G.; Benner, R. What happens to terrestrial organic matter in the ocean? *Org. Geochem.* **1997**, *27*, 195–212. [CrossRef]
76. Gan, S.; Wu, Y.; Zhang, J. Bioavailability of dissolved organic carbon linked with the regional carbon cycle in the East China Sea. *Deep. Res. Part II* **2016**, *124*, 19–28. [CrossRef]
77. Alldredge, A.L.; Cowles, T.J.; MacIntyre, S.; Rines, J.E.; Donaghay, P.L.; Greenlaw, C.F.; Holliday, D.V.; Dekshenieks, M.M.; Sullivan, J.M.; Zaneveld, J.R. Occurrence and mechanisms of formation of a dramatic thin layer of marine snow in a shallow Pacific fjord. *Mar. Ecol. Prog. Ser.* **2002**, *233*, 1–12. [CrossRef]
78. Kang, K.H.; Shin, H.S.; Park, H. Characterization of humic substances present in landfill leachates with different landfill ages and its implications. *Water Res.* **2002**, *36*, 4023–4032. [CrossRef]
79. He, W.; Bai, Z.; Li, Y.; Kong, X.; Liu, W.; Yang, C.; Yang, B.; Xu, F. Advances in environmental behaviors and effects of dissolved organic matter in aquatic ecosystems. *Sci. Sin. Terrae* **2016**, *46*, 341–355. [CrossRef]
80. Druffel, E.R.; Williams, P.M.; Bauer, J.E.; Ertel, J.R. Cycling of dissolved and particulate organic matter in the open ocean. *J. Geophys. Res. Oceans* **1992**, *97*, 15639–15659. [CrossRef]
81. Wei, H.; Cai, J.; Wang, G.; Wang, X. The diversity of organic matter in marine sediments and the suspiciousness of source parameters: A review. *Adv. Earth Sci.* **2018**, *33*, 1024–1033.
82. Cai, J.; Zeng, X.; Wei, H.; Song, M.; Wang, X.; Liu, Q. From water body to sediments: Exploring the depositional processes of organic matter and their implications. *J. Palaeogeogr.* **2019**, *21*, 49–67.
83. Tissot, B.; Durand, B.; Espitalié, J.; Combaz, A. Influence of nature and diagenesis of organic matter in formation of petroleum. *AAPG Bull.* **1974**, *58*, 499–506.
84. Lewan, M.D. Hydrous pyrolysis. In *Encyclopedia of Petroleum Geoscience*; Sorkhabi, R., Ed.; Springer International Publishing: New York, NY, USA, 2017; pp. 1–7.
85. Loucks, R.G.; Ruppel, S.C. Mississippian Barnett Shale: Lithofacies and depositional setting of a deep-water shale-gas succession in the Fort Worth Basin, Texas. *AAPG Bull.* **2007**, *91*, 579–601. [CrossRef]
86. Loucks, R.G.; Reed, R.M.; Ruppel, S.C.; Jarvie, D.M. Morphology, genesis, and distribution of nanometer-scale pores in siliceous mudstones of the Mississippian Barnett shale. *J. Sediment. Res.* **2009**, *79*, 848–861. [CrossRef]

87. Loucks, R.G.; Reed, R.M.; Ruppel, S.C.; Hammes, U. Spectrum of pore types and networks in mudrocks and a descriptive classification for matrix-related mudrock pores. *AAPG Bull.* **2012**, *96*, 1071–1098. [CrossRef]
88. Reed, R.M.; Loucks, R.G.; Ko, L.T. Scanning electron microscopic petrographic differentiation among different types of pores associated with organic matter mudrocks. *GCAGS J.* **2020**, *9*, 17–27.